Cell Reports

Resource

Massively Parallel Single Nucleus Transcriptional Profiling Defines Spinal Cord Neurons and Their Activity during Behavior

Graphical Abstract

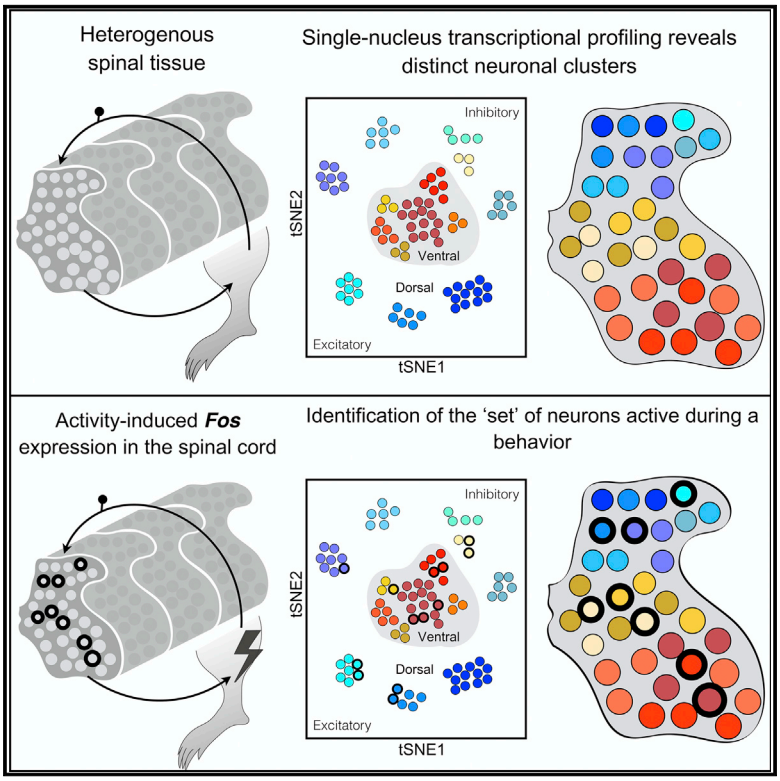

Authors

Anupama Sathyamurthy, Kory R. Johnson, Kaya J.E. Matson, ..., Michael C. Kelly, Matthew W. Kelley, Ariel J. Levine

Correspondence

ariel.levine@nih.gov

In Brief

Sathyamurthy et al. use massively parallel single nucleus RNA-seq to probe spinal cord cell types and present an atlas of 43 neuronal populations. By using this approach after a sensory and a motor behavior, they were able to detect and molecularly identify activated neurons associated with each function.

Highlights

- An atlas of adult mouse spinal cord cell types
- A resource of the molecular repertoires of 43 neuronal populations
- A simple method using snRNA-seq to identify activated neurons following behavior

Data and Software Availability

GSE103892

Sathyamurthy et al., 2018, Cell Reports *22*, 2216–2225
February 20, 2018
https://doi.org/10.1016/j.celrep.2018.02.003

CellPress

OPEN ACCESS
CellPress

Cell Reports
Resource

Massively Parallel Single Nucleus Transcriptional Profiling Defines Spinal Cord Neurons and Their Activity during Behavior

Anupama Sathyamurthy,[1,4] Kory R. Johnson,[2,4] Kaya J.E. Matson,[1] Courtney I. Dobrott,[1] Li Li,[1] Anna R. Ryba,[1] Tzipporah B. Bergman,[1] Michael C. Kelly,[3] Matthew W. Kelley,[3] and Ariel J. Levine[1,5,*]

[1]Spinal Circuits and Plasticity Unit, National Institute of Neurological Disorders and Stroke, Bethesda, MD 20892, USA
[2]Bioinformatics Section, Information Technology Program, National Institute of Neurological Disorders and Stroke, Bethesda, MD 20892, USA
[3]Laboratory of Cochlear Development, National Institute on Deafness and Other Communication Disorders, Bethesda, MD 20892, USA
[4]These authors contributed equally
[5]Lead Contact
*Correspondence: ariel.levine@nih.gov
https://doi.org/10.1016/j.celrep.2018.02.003

SUMMARY

To understand the cellular basis of behavior, it is necessary to know the cell types that exist in the nervous system and their contributions to function. Spinal networks are essential for sensory processing and motor behavior and provide a powerful system for identifying the cellular correlates of behavior. Here, we used massively parallel single nucleus RNA sequencing (snRNA-seq) to create an atlas of the adult mouse lumbar spinal cord. We identified and molecularly characterized 43 neuronal populations. Next, we leveraged the snRNA-seq approach to provide unbiased identification of neuronal populations that were active following a sensory and a motor behavior, using a transcriptional signature of neuronal activity. This approach can be used in the future to link single nucleus gene expression data with dynamic biological responses to behavior, injury, and disease.

INTRODUCTION

To understand how networks of cells mediate behavior, it is necessary to classify the various cell types of the brain, spinal cord, and peripheral nervous system and to know which populations of cells are involved in specific functions. Gene expression-based definitions of cell identity have been a foundation of spinal cord biology for the past 30 years. In particular, the use of post-natal genetic markers to control defined classes of spinal cord neurons has enabled the functional characterization of many cell types and has advanced our understanding of how these populations contribute to normal sensory-motor behavior (Abraira et al., 2017; Azim et al., 2014; Bikoff et al., 2016; Bourane et al., 2015; Dougherty et al., 2013; Duan et al., 2014; Hilde et al., 2016; Koch et al., 2017b; Mishra and Hoon, 2013; Peirs et al., 2015; Satoh et al., 2016; Sun et al., 2009). However, there are three important limitations to this approach. First, there is no census of neuronal cell types in the adult spinal cord. The lack of such a resource limits the application and interpretation of genetic manipulations, and it is not known how previously described cell types relate to one another. Second, the unique gene expression profiles that endow cell types with their functional repertoires are not known. Third, we lack an unbiased approach to identify the set of spinal cord cell types associated with a given neural function, such as motor behavior or the response to a sensory stimulus.

Pioneering work using massively parallel single-cell sequencing has established that a cell's transcriptional program is a powerful strategy for defining cell type (Campbell et al., 2017; Chen et al., 2017; Jaitin et al., 2014; Lake et al., 2016; Li et al., 2016; Macosko et al., 2015; Shin et al., 2015; Tasic et al., 2016; Usoskin et al., 2015; Villani et al., 2017). Furthermore, single-cell RNA sequencing has been adapted to provide unbiased detection of immediate-early gene expression in molecularly defined cell types following seizure, acute anxiety, or sensory experience in the striatum and visual cortex (Hrvatin et al., 2018; Wu et al., 2017).

We sought to develop an approach that simultaneously provides a single-cell gene expression census of the cell types of the adult spinal cord and the ability to overlay a map of the transcriptional signature of neuronal activity following behavior. To characterize the gene expression and cell-type composition of the adult mouse spinal cord, we used massively parallel single nucleus RNA-seq (snRNA-seq). We created a catalog of spinal cord neuronal cell types, characterizing 43 classes of neurons. Analysis of the genes expressed in each cell type provided a powerful resource for understanding the mechanistic basis of functional neuronal heterogeneity. This work also revealed distinct organizing principles for molecular heterogeneity between neuronal populations in the dorsal and ventral horns. To provide unbiased characterization of the classes of spinal neurons that were associated with defined behaviors, we performed this technique immediately following a painful sensory stimulation or a locomotor behavior. This approach could be used to reveal comprehensive single nucleus response maps for a range of behaviors and disease states, establishing an unprecedented

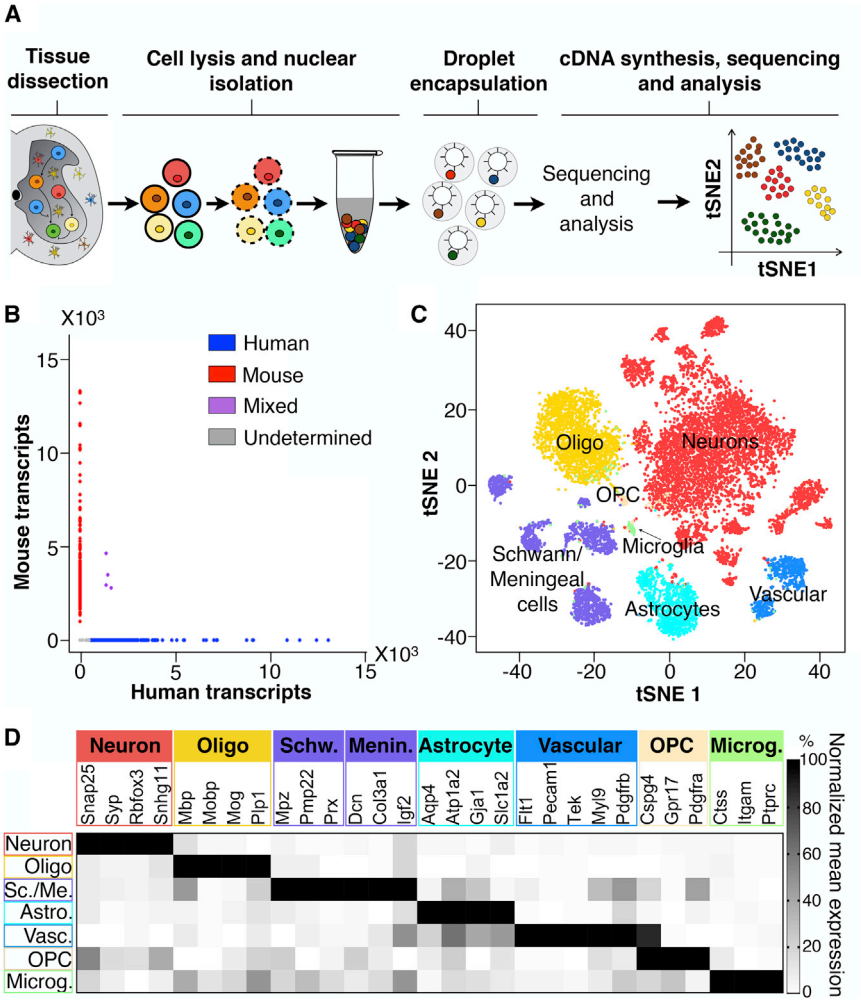

Figure 1. Massively Parallel snRNA-Seq Was Used to Define Cell Types in the Adult Mouse Spinal Cord

(A) Summary of experimental strategy.

(B) Barnyard plot of pooled human and mouse spinal cord nuclei showing beads that were associated with human transcripts, mouse transcripts, both human and mouse transcripts (mixed), or those that could not be determined (undetermined).

(C) tSNE visualization plot of 17,354 spinal cord nuclei, colored according to seven major SC3-defined clusters: neurons, oligodendrocytes (oligos), meningeal and Schwann cells, astrocytes, vascular cells, oligodendrocyte precursor cells (OPCs), and microglia.

(D) Heatmap of normalized mean expression for key marker genes for each major SC3-defined cluster.

See also Figure S1 and Table S1.

link between single nucleus gene expression and circuit- and system-level function within the spinal cord.

RESULTS

snRNA-Seq Identification of Major Spinal Cord Cell Types

To adapt massively parallel RNA sequencing approaches to the spinal cord, we opted to perform single nucleus, rather than single cell, analysis for three key reasons: single nucleus transcriptional profiling accurately permits cell-type analysis, avoids experimental artifacts from transcriptional changes induced in intact cells during the tissue dissociation process, and can be performed easily from whole tissue, including tissue that is difficult to dissociate (such as the spinal cord), frozen material, and human biobank material (Grindberg et al., 2013; Habib et al., 2017; Lake et al., 2016, 2017; Matevossian and Akbarian, 2008).

To establish an snRNA-seq strategy for the adult spinal cord, we used a detergent-based protocol, which allowed rapid and thorough nuclear release and transfer of the material to cold temperatures, thereby minimizing gene expression changes (Figure 1A; Figure S1A). Nuclei were easily isolated from adult mouse spinal cord and frozen adult human spinal cord. We next sought to modify Drop-Seq (Macosko et al., 2015), a droplet-based approach for massively parallel single-cell RNA capture, cDNA synthesis, and sequencing, to allow this technique to be used for single nuclei. We found that simply increasing the concentration of detergent in the Drop-Seq lysis buffer improved nuclear lysis and generated smaller droplets than standard Drop-Seq (mean 0.48 ± 0.06 nL SEM) (Figures S1B–S1D). To determine whether this approach enables single nucleus droplet encapsulation, nuclei from human spinal cord were pooled with nuclei from mouse spinal cord, and we examined how many beads contained both human and mouse transcripts (Figure 1B). We found that 2% of droplets with a mouse nucleus also contained a human nucleus (4/196 mouse nuclei), which represents a calculated doublet rate of 4.1%. Thus, single nuclei can be obtained from difficult-to-dissociate and frozen human spinal cord tissue and can be processed through Drop-Seq with a simple buffer modification.

Using this approach, we sequenced and analyzed 17,354 nuclei from adult mouse lumbar spinal cord. We found seven major clusters that corresponded to the following cell types, based on marker expression: neurons (52% of total nuclei), oligodendrocytes (16% of total nuclei), a mixed population of meningeal and Schwann cells (14% of total nuclei), astrocytes (9% of total nuclei), vascular cells (5% of total nuclei), oligodendrocyte precursor cells (1% of total nuclei), and microglia (1% of total nuclei) (Figure 1D; Figure S1E; Table S1). The diversity of the RNA transcript yield that we obtained, reflected in the number of genes per nucleus, varied among cell types (Figure S1F).

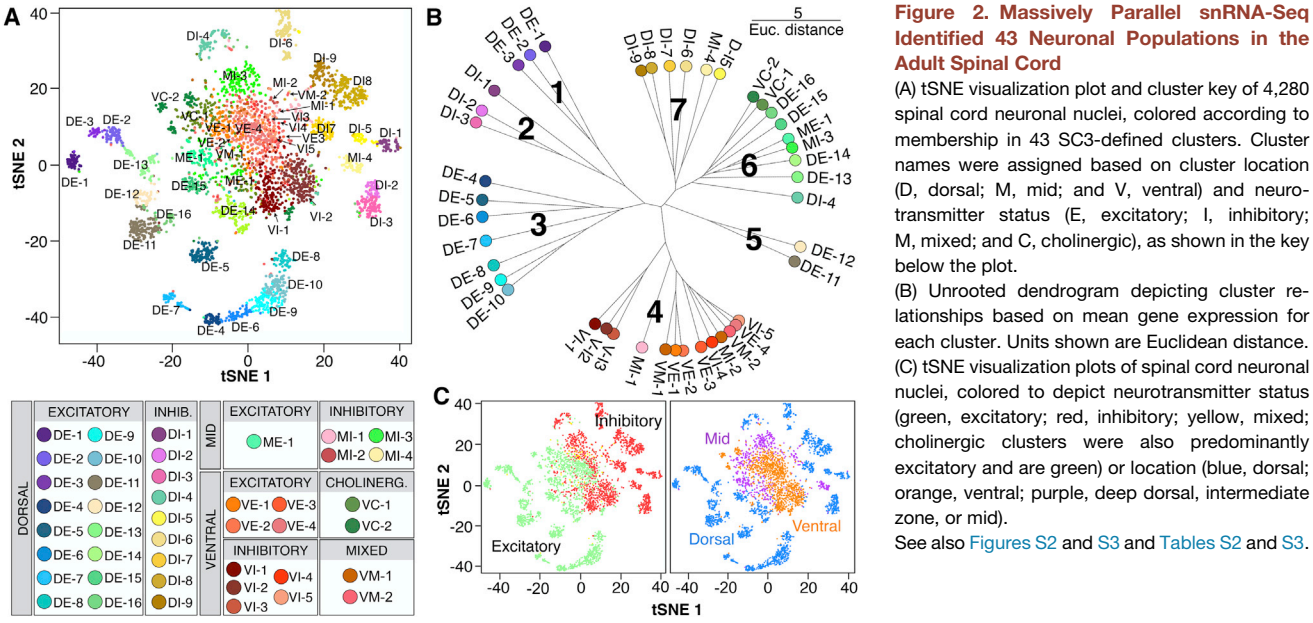

Figure 2. Massively Parallel snRNA-Seq Identified 43 Neuronal Populations in the Adult Spinal Cord

(A) tSNE visualization plot and cluster key of 4,280 spinal cord neuronal nuclei, colored according to membership in 43 SC3-defined clusters. Cluster names were assigned based on cluster location (D, dorsal; M, mid; and V, ventral) and neurotransmitter status (E, excitatory; I, inhibitory; M, mixed; and C, cholinergic), as shown in the key below the plot.

(B) Unrooted dendrogram depicting cluster relationships based on mean gene expression for each cluster. Units shown are Euclidean distance.

(C) tSNE visualization plots of spinal cord neuronal nuclei, colored to depict neurotransmitter status (green, excitatory; red, inhibitory; yellow, mixed; cholinergic clusters were also predominantly excitatory and are green) or location (blue, dorsal; orange, ventral; purple, deep dorsal, intermediate zone, or mid).

See also Figures S2 and S3 and Tables S2 and S3.

Census of Adult Spinal Cord Neuronal Populations

To identify and characterize neuronal classes within the adult mouse spinal cord, 4,280 neuronal nuclei were analyzed and partitioned into 43 clusters (Figure 2A; Figure S2A; Table S2). We first characterized the neurotransmitter status, a core feature of neuronal identity, of each cluster by analyzing excitatory, inhibitory, and cholinergic marker expression. We found that 53% of neuronal nuclei were in 23 predominantly excitatory clusters (including 2 cholinergic clusters), 45% were in 18 predominantly inhibitory clusters, and 2.5% were in 2 clusters with both excitatory and inhibitory markers (Figure S3A). Within this latter group, only rare individual neuronal nuclei co-expressed excitatory and inhibitory markers (n = 2/109), which may reflect doublets and cannot account for the substantial fractions of excitatory and inhibitory marker-expressing nuclei in these clusters. Therefore, these two clusters contained separate excitatory and inhibitory populations that share overall similar gene expression.

Next, we analyzed relationships between clusters by performing Euclidean-based hierarchical clustering on the mean expression of each gene in each cluster (Figure 2B). A dendrogram presentation of these relationships revealed seven major groupings, five of which shared a common neurotransmitter status (groups 1, 2, 3, 5, and 7) (Figure 2B). To determine what other parameters are major organizing features of neuronal populations, we compared all genes that significantly contributed to defining any cluster with public gene expression databases (Gong et al., 2003; Lein et al., 2007). This allowed us to probe the cluster distribution of previously known marker genes (Figure S3B) and to determine the spatial location of each cluster. We found that 55% of neuronal nuclei were in 25 dorsal clusters, 34% were in 13 ventral clusters, and 11% were in 5 clusters in the deep dorsal horn or intermediate zone. Four of seven major dendrogram groupings each had a common regional location within the spinal cord (groups 1, 2, 3, and 5) (Figure 2B). To further analyze neurotransmitter status and spatial location across clusters, each population was colored by these features and plotted by t-distributed stochastic neighbor embedding (tSNE) analysis (Figure 2C). The structure of the tSNE distribution of neurons according to these parameters supported the importance of location and neurotransmitter status as defining features of spinal cord cell types. Accordingly, clusters were named by their spatial location (D, dorsal; V, ventral; or M, deep dorsal, intermediate, or "mid" cord) and their neurotransmitter status (E, excitatory; I, inhibitory; M, mixed; C, cholinergic) (Figure 2).

A major difference in cluster organization was observed between dorsal and ventral clusters. tSNE visualization revealed that dorsal clusters form an outer ring of discrete groups while ventral clusters overlapped one another in the center of the plot, with deep dorsal and intermediate clusters between (Figure 2C). Similarly, dorsal clusters were generally present as homogeneous blocks in a cell consensus matrix and had high SC3 silhouette width consensus values (a measure that represents the diagonality of the matrix), while ventral clusters showed inter-relatedness with other ventral clusters and had low silhouette width consensus values (Figure S2). At a molecular level, markers for ventral clusters were often shared across ventral populations (as explained later). These differences were not based on a failure to segregate ventral neurons due to low molecular information content, because the number of genes per nucleus was 2,465 ± 202 in ventral neurons and 1,346 ± 33 in dorsal neurons (mean ± SEM). This analysis suggests a general principle that the dorsal horn of the spinal cord contains more molecularly distinct populations while the ventral horn displays overlapping gene expression patterns.

We next sought to determine what categories of genes drive neuronal diversity. Gene ontology (GO) term analysis of the

A

Molecular function	Enrichment score
Glutamate receptor activity	4.2
Potassium channel activity	3.01
Transcriptional regulator	2.86
cAMP signaling	2.04
Transcriptional regulator	1.68
Gaba receptor/Cl channel activity	1.65
Acetylcholine receptor activity	1.52

B

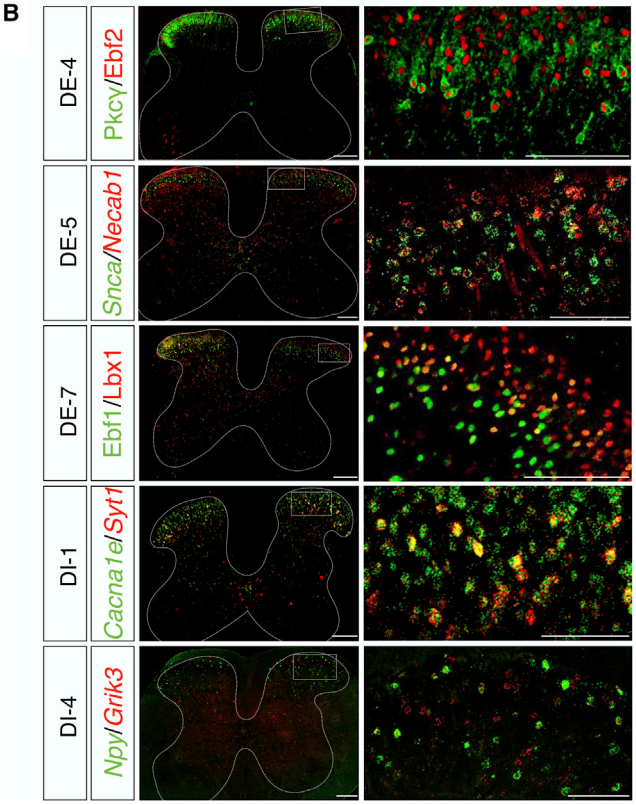

Figure 3. Gene Expression that Defined Spinal Cord Neuronal Populations

(A) Summarized GO terms that were significantly enriched (>1.3 enrichment score) among the top genes associated with each cluster.

(B) Validation co-labeling for pairs of cluster-defining genes using immunofluorescence (DE-4 and DE-7) or fluorescent *in situ* hybridization (DE-5, DI-1, and DI-4). Images taken at 20×, with the full image (scale bar, 200 μm) and magnification (scale bar, 100 μm) shown in the left and right panels of each pair, respectively.

See also Figure S3 and Table S3.

top genes associated with each cluster was performed. We found that neurotransmitter receptors and ion channels, transcription factors, and cyclic AMP (cAMP) signal transduction components are significantly over-represented among the top genes that contribute to defining these clusters (Figure 3A). Many genes within these molecular function families were enriched or specifically expressed in particular populations or related groups (Figures S3C–S3E).

To identify candidate marker genes for the 43 clusters, and to characterize their gene expression profiles, we further analyzed all genes that significantly contributed to defining each cluster. Many clusters were partially defined by previously established markers (Figure S3B) (Abraira et al., 2017; Bikoff et al., 2016; Koch et al., 2017a; Lu et al., 2015; Todd, 2017), and in most of these clusters, we identified new key genes (Figures 3B and 4). In addition, we identified previously unrecognized cell populations (Figure 4). Table S3 is a searchable database of the mean gene expression and the percent cluster membership for each gene. This provides the opportunity to probe the molecular identity of each population or to search across clusters for a gene of interest. A summary of each group of clusters with highlighted findings follows.

Group 1 was composed of the dorsal excitatory (DE) clusters DE-1–DE-3. These clusters shared expression of the transcription factor *Ebf2* (together with DE-4–DE-7) and the γ-aminobutyric acid (GABA) receptor *Gabrg3.* They were peptidergic, expressing the enzyme *Pam* and the genes for neuropeptides *Grp* and/or *Sst.* DE-1 expressed the mu opioid receptor *Oprm1*, DE-2 expressed the peptide receptor *Npy1r*, and DE-3 expressed *Ntrk2*/TrkB.

Group 2 was composed of the dorsal inhibitory (DI) clusters DI-1–DI-3. These clusters shared expression of the peptide receptor *Sstr2*, as well as the glutamate receptor *Grik2* and the potassium channel *Kcnc2.* DI-1 expressed *Calb2*/calretinin, and DI-2 and DI-3 were peptidergic, expressing the enzyme *Pam* and the genes for *Gal* (DI-2) and *Pnoc*/nociception (DI-3), as well as *Nos1* (DI-3).

Group 3 was composed of the DE clusters DE-4–DE-10. There were two subgroups. DE-4–DE-7 expressed *Ebf2* (together with DE-1–DE-3) and *Calb1*/calbindin and were peptidergic, expressing *Pam*, as well as *Sst*/SOM (DE-4 and DE-5), *Tac2*/NeurokininA (DE-5), *Calca*/CGRP (DE-5), *Nts*/neurotensin (DE-6), *Penk*/enkephalin (DE-6), and *Cck* (DE-7). DE-4 also expressed *Prkcg*/PKCγ. DE-8–DE-10 expressed the transcription factor *Maf* and were not peptidergic. DE-8 expressed *Cbln2*, DE-9 expressed *Adarb2*, and DE-10 expressed enriched levels of *Slc17a8*/vGlut3.

Group 4 was composed of the ventral inhibitory (VI) clusters VI-1–VI-5, ventral excitatory (VE) clusters VE-1–VE-4, ventral mixed (VM) clusters VM-1 and VM-2, and mid inhibitory (MI) deep dorsal clusters MI-1 and MI-2. Overall, this group shared expression of the transcription factors *Esrrg*/ERRγ and Foxp2, as well as the sodium channel *Scn1a*, which has been shown to correlate positively with maximum firing rate (Tripathy et al., 2017). Several ventral clusters (VI-1, VI-4, VI-5, VE-3, and VE-4) and MI-2 also shared expression of the peri-neuronal net components *Acan* and *Bcan* and the link protein *Hapln1.* This is consistent with the observation that peri-neuronal nets have been shown to surround many previously unidentified ventral neurons (Galtrey et al., 2008). Cluster VI-5 was also distinguished by being enriched for nearly all genes associated with the mammalian target of rapamycin (mTOR) complexes mTORC1 and mTORC2 that

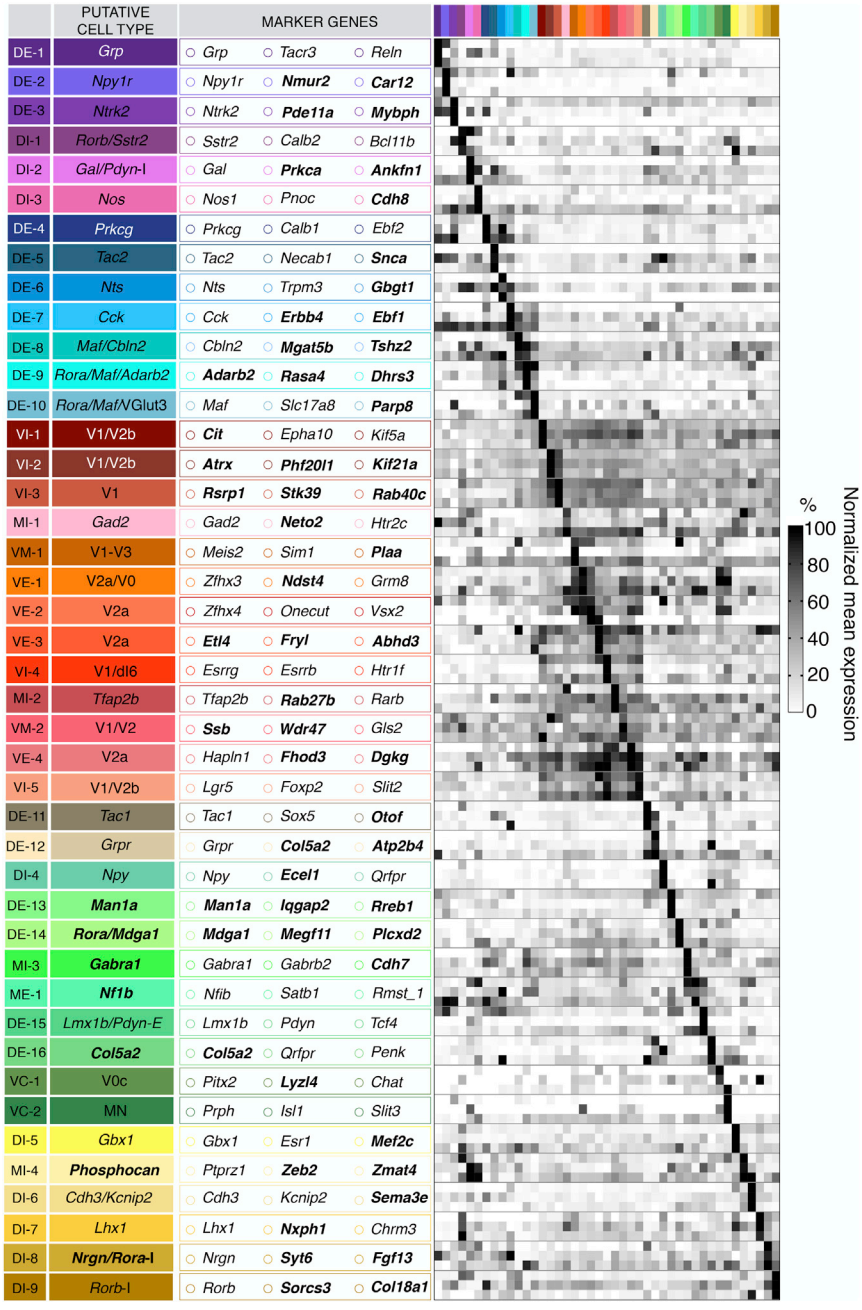

Figure 4. Summary of 43 Spinal Cord Neuronal Populations

For each population, the cluster name, a putative cell-type assignment, and key marker genes are shown. Previously undescribed cell types and markers are shown in bold. The expression of the marker genes across clusters are shown as a heatmap of normalized mean gene expression. See also Table S3.

play key roles in cell metabolism and survival (Laplante and Sabatini, 2012), including *Mtor*/mTOR, *Rptor*/RAPTOR, *Mlst8*/GβL, *Deptor*, *Rictor*, and *Mapkap1*/SIN1, as well as the mTOR pathway regulators *Rheb*, *Tsc1*, and *Tsc2*. Surprisingly, many embryonic and early postnatal ventral cell fate markers were found within these clusters and may provide a link between the embryonic lineage-defined identity and the adult populations described here (Figure S3F) (Alvarez et al., 2005; Bikoff et al., 2016; Catela et al., 2015; Lu et al., 2015; Perry et al., 2015; Seredick et al., 2014). As examples, VE-1–VE-3 were enriched for embryonic lineage V2a markers, including *Vsx2*/Chx10, *Shox2*, *Lhx3*, and *Lhx4*, and cluster VI-4 was enriched for the embryonic lineage dI6 markers *Wt1* and *Dmrt3* and the embryonic lineage V1-subtype markers *Chrna2* (Renshaw), *Pvalb* (1a inhibitory interneurons), and *Esrrb*/Nr3b2. However, many of these embryonically expressed genes had very low expression levels in these clusters, and even for the genes with stronger expression, it is not certain whether the same cells continue to express these genes from embryonic through adult stages.

Group 5 was composed of the DE clusters DE-11 and DE-12, which shared expression of the transcription factor *Sox5* and the potassium channel *Kcnd3.* DE-11 was peptidergic, expressing *Pam*, *Penk*, and *Tac1*/substance P, while DE-12 was not peptidergic but expressed the peptide receptor *Grpr.*

Group 6 was composed of a diverse collection of clusters: DI-4, DE-13–DE-16, MI-3, mid excitatory (ME) cluster ME-1, and ventral cholinergic (VC) clusters VC-1 and VC-2. Clusters DI-4 and DE-13–DE-16 are peptidergic, expressing *Npy* (DI-4), *Calca*/CGRP (DE-13), *Cck* and *Tac1*/substance P (DE-14), *Pdyn*/dynorphin (DE-15), and *Penk*/enkephalin (DE-16). VC-1 expressed the embryonic lineage $V0_c$ marker *Pitx2.* VC-2 expressed markers of spinal motoneurons, including *Prph*/peripherin, *Isl1*, *Map1b*, *Nrg1*, and *Slit3*, as well as *Nkain1*, which has been shown to correlate positively with input resistance (Tripathy et al., 2017).

Group 7 was composed of the DI clusters DI-5–DI-9 and the deep dorsal cluster MI-4 that shared expression of the glutamate receptor *Grik2.* These clusters expressed previously described DI transcription factors *Gbx1* (DI-5), *Lhx1* (DI-7), and *Rorb* (DI-9). DI-5 also expressed the estrogen receptor *Esr1*, DI-6 expressed *Cdh3* and *Kcnip2*, and DI-8 expressed *Nrgn*/Neurogranin.

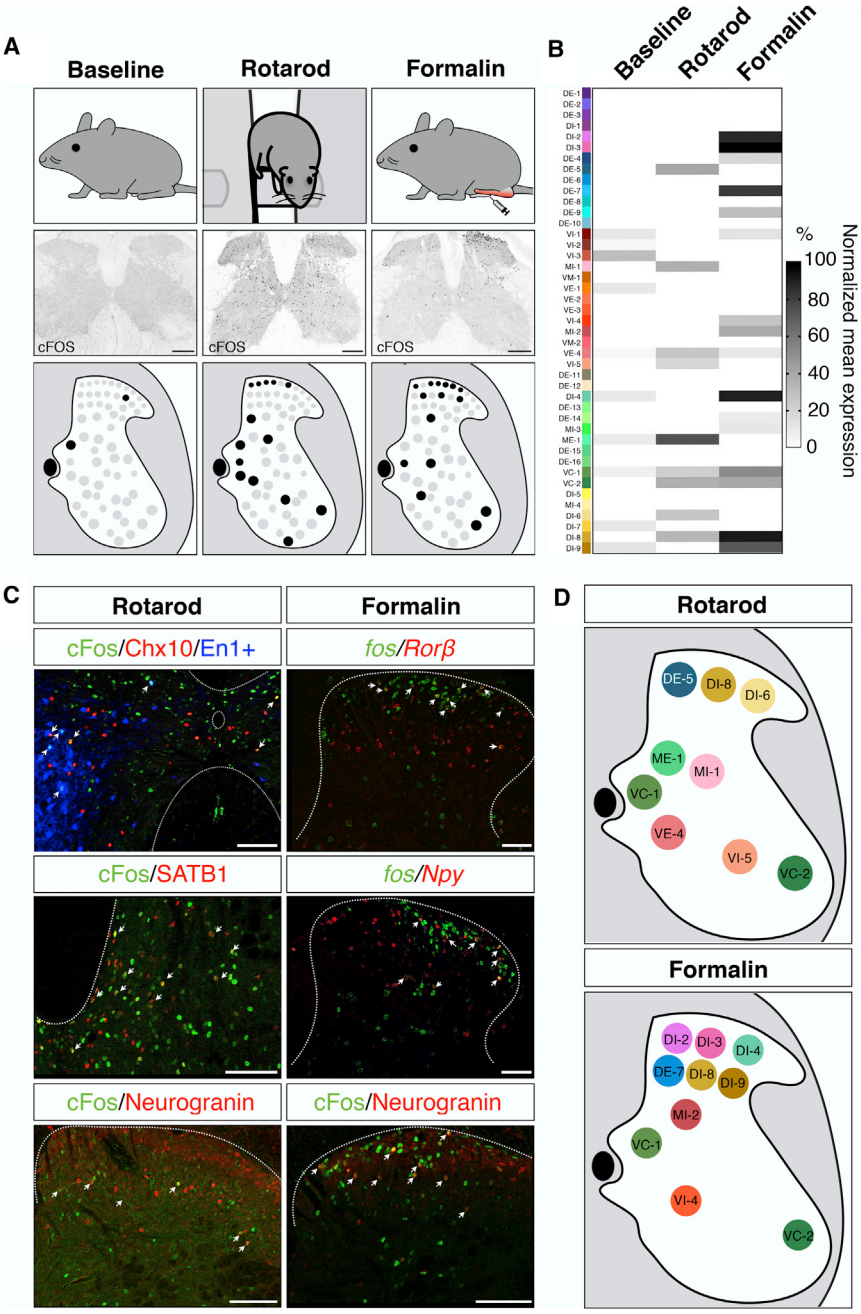

Figure 5. snRNA-Seq Identified Active Neurons Following Behavior

(A) Characteristic pattern of cFOS expression at baseline, following rotarod locomotion or after formalin injection in the hindpaw, at 60 min following behavior.

(B) *Fos* RNA expression as detected by snRNA-seq across clusters in baseline, rotarod, and formalin samples, shown as normalized mean gene expression per cluster.

(C) Experimental validation of clusters associated with each behavior, as detected by snRNA-seq. For each cluster, a marker gene was compared with cFOS protein expression by immunofluorescence (En1:Cre;Ai9/Chx10, Satb1, and Neurogranin) or *Fos* RNA by fluorescent *in situ* hybridization (*Rorb* and *Npy*) (scale bars, 100 μm).

(D) Summary of the set of neuronal populations associated with each behavior, as identified by snRNA-seq.

See also Figure S4.

Collectively, these 43 clusters establish an atlas of spinal cord neuronal populations and their constituent molecules.

snRNA-Seq Following Behavior Identified Active Neurons

Having characterized the spinal cord neuron populations, we next considered that snRNA-seq could provide an unbiased, cell-type based characterization of neurons that express immediate-early genes following a behavioral paradigm. We found that direct isolation of nuclei did not induce *Fos* RNA (Figure S1A) but that detectable *Fos* expression in nuclei could be induced 5 min following a painful sensory stimulus (formalin hindpaw injection) (Figure S4). To determine whether *Fos* RNA can be detected at the single nucleus level following behavior, snRNA-seq was performed following formalin injection or rotarod locomotion. *Fos* was expressed in a higher proportion of nuclei following rotarod locomotion (1.6%) or formalin administration (1.9%) compared with baseline (0.48%), and the level of *Fos* gene expression was significantly increased (0.0082 ± 0.0025 counts per million (cpm) after rotarod, 0.0175 ± 0.0040 cpm after formalin, and 0.0024 ± 0.0009 cpm at baseline; mean ± SEM; $p < 0.001$, ANOVA, corrected p value). Thus, massively parallel snRNA-seq following behavior detected a transcriptional signature of neuronal activity.

Next, we used the distribution of *Fos* RNA expression to map neuronal activity across clusters following rotarod locomotion or formalin administration, because these experimental paradigms produce classic patterns of cFOS protein expression (Figure 5A) (Herdegen et al., 1994; Jasmin et al., 1994). During locomotion, each of the major ventral embryonic lineage domains gives rise to neurons that are important for specific features of locomotion, such as flexor and extensor alternation (V1- and V2b-derived cells) and left and right alternation (V2a-derived cells) (Crone et al., 2008; Zhang et al., 2014). In addition, cholinergic interneurons express cFOS protein following locomotion in cat, and these may correlate with $V0_c$ neurons (Huang et al., 2000; Zagoraiou et al., 2009). However, the identities of locomotor-associated intermediate and dorsal horn neurons are not well established, with the exceptions of protein kinase C gamma

(PKCγ)-expressing neurons in the rat (Neumann et al., 2008) and *Rorb*-expressing neurons (Koch et al., 2017b). We hypothesized that the application of snRNA-seq following rotarod running would help to reveal the set of adult neurons that are active during locomotion.

Following locomotion, *Fos* RNA was detected in ventral clusters VC-1 (which includes Pitx2-expressing $V0_c$ neurons), VC-2 (spinal motoneurons), VE-4 (which includes putative V2a neurons) and VI-5 (which includes putative V1/V2b neurons), thereby confirming that these cell types are associated with locomotion (Figure 5B). We used markers to validate this approach and found that VE-4 (Chx10) and VI-5 cells (En1:Cre;Ai9) express cFOS after rotarod locomotion (Figure 5C). Within the intermediate zone and dorsal horn, clusters ME-1, MI-1, DE-5, DI-6, and DI-8 expressed *Fos* RNA, but we did not detect *Fos* RNA in cluster DE-4 that expresses *Prkcg*/PKCγ (Figure 5B). This may be due to species differences or a technical false negative. *Rorb* expression is highest in cluster DI-9, which was not detected using this approach, but it is also present in cluster DI-8, which did express *Fos* after locomotion. Using markers for clusters ME-1 (Satb1) and DI-8 (Nrgn), we confirmed that these newly defined clusters express cFOS protein after locomotion, thereby expanding the known set of neuronal populations that are associated with this core behavior (Figure 5D).

Formalin administration is a well-established pain assay, and it has previously been shown to activate predominantly dorsal horn spinal cord neurons, including those that express *Gal*, *Sstr2*, *Nos1*, *Npy*, *Penk*, and *Tacr1*/Nk1r, creating specific expectations for which clusters should be detected (Herdegen et al., 1994; Hossaini et al., 2010; Lee et al., 1993; Polgár et al., 2013). Following formalin injection, *Fos* RNA was observed in clusters DI-2 (which includes Gal and Sstr2-expressing neurons), DI-3 (which includes Nos1-expressing neurons), and DI-4 (which includes Npy-expressing neurons), confirming that these neurons express *Fos* after formalin administration, as well as DI-8, DI-9, DE-7, VI-4, VC-1, VC-2, and MI-2 (Figure 5C). *Penk* and *Tacr1*/Nk1r are both distributed across several clusters. We used markers for clusters DI-4 (Npy), DI-8 (Nrgn), and DI-9 (Rorb) to validate these findings and found that these populations express *Fos* RNA or cFOS protein following formalin administration (Figure 5C). Thus, in both a sensory test and a motor behavior, massively parallel snRNA-seq provided an unbiased definition of cell types that displayed activity-induced transcription and revealed new cell types that are associated with each function.

DISCUSSION

The spinal cord plays essential roles in sensory processing and motor control, but how the cells of the cord function together in networks to mediate behavior is not well understood. Here, we sought to identify spinal cord cell types and their contributions to behavior through single nucleus transcriptional profiling. Massively parallel snRNA-seq was used to analyze more than 17,000 nuclei from the adult mouse spinal cord. We created an atlas of spinal cord neuronal populations, characterizing 43 cell types. By applying snRNA-seq following behavior, we detected transcriptional signatures of neuronal activity and identified neuronal populations associated with a sensory and a motor function.

We have described 43 neuronal populations within the adult mouse lumbar spinal cord, including previously unrecognized cell types. This work establishes a cellular framework for the spinal cord and facilitates the comparison and integration of prior work that generally used single markers to define cell types. We detected clusters that correspond to nearly all previously described adult spinal cord neuronal populations, with the primary exceptions being populations that were previously described by a single marker gene that is expressed more broadly within the spinal cord (such as *Penk* and *Pvalb*).

The perspective afforded by massively parallel single nucleus sequencing also revealed an intriguing difference between dorsal and ventral neuronal populations. We found that dorsal neuron types were more distinct from one another, forming discrete clusters, while ventral neuron types were more closely associated with one another. Previously, most analysis of spinal cord cell types emphasized adult molecular markers in the dorsal horn and embryonic lineage domain-defined cell types in the ventral horn. Together with our findings, this may reflect different organizing principles for neuronal identity in the dorsal and ventral spinal cord. It is possible that in the adult spinal cord, cellular identity in the dorsal horn is governed by restricted and ongoing expression of genes for specific cellular functions, whereas in the ventral horn, it is governed by factors defined during development, such as cell location, axon guidance, and genetically programmed synaptic specificity.

This work also reveals the molecular repertoire of each neuronal population, providing a significant extension of our understanding of spinal cord cell types. The searchable database that is included here (Table S3) will allow researchers to probe the complement of genes in cell types of interest and analyze the expression of genes of interest across clusters. This will serve as a powerful tool to advance our understanding of the molecular mechanisms that mediate functional heterogeneity among neuronal populations.

Despite the strengths of this work, three major limitations must be noted. First, we detected a lower number of genes per nucleus than is typically detected from whole cells or nuclei (Grindberg et al., 2013; Habib et al., 2016, 2017; Lacar et al., 2016; Lake et al., 2016; Macosko et al., 2015). This is likely due to several factors, including the lower amount of RNA in the nucleus compared with the whole cell, the trade-off between resolution and scale for low-throughput versus massively parallel approaches, technical differences such as mRNA capture and reverse transcription efficiency, and cell-type differences. Despite this first limitation, we obtained a sufficient number of genes per nucleus to permit successful clustering of neuronal populations. A second major limitation is that this work only characterized the cell types of the lumbar spinal cord. Although the major classes of known cell types are present along the full rostro-caudal axis of the spinal cord, work has revealed that distinct subpopulations may vary at different segmental levels (Francius et al., 2013; Hayashi et al., 2018; Sweeney et al., 2018). Accordingly, future work is necessary to fully characterize spinal cord cell types outside of the lumbar region. A third major limitation is that the use of snRNA-seq for

activity profiling can only identify cells that induced a transcriptional response above a detection threshold. As a result, this approach will not detect all neural activity, and negative results must be interpreted with caution.

Massively parallel single nucleus transcriptional profiling has the potential to reveal unprecedented knowledge about cell types, the transcriptional programs of cell types, and gene expression control in an array of *in vivo* settings in animal models. With this resource in hand, single nucleus transcriptional profiling can be used to probe spinal cord neuronal and non-neuronal responses to disease or injury, to study how the molecular and cellular composition of a tissue changes over time, and to reveal the selective loss of cell types during degeneration or gain of cell types during inflammation. Because nuclei are readily obtained from human patient-derived and archived bio-bank material, snRNA-seq can be applied to study human biology as well (Habib et al., 2017; Lake et al., 2016; Matevossian and Akbarian, 2008). We now have the tools to reach a new level in our understanding of the molecular and cellular mechanisms by which complex tissues mediate basic function, behavior, and disease.

EXPERIMENTAL PROCEDURES

Mice and Behavior

All animal work was performed in accordance with a protocol approved by the National Institute of Neurological Disorders and Stroke Animal Care and Use Committee. Balanced samples of male and female ICR/CD-1 wild-type mice, between 8 and 12 weeks old, were used for all experiments except those shown in Figure 5C, for which En1:Cre;Ai9 mice (Stock No. 007916 × Stock No. 007909, both from The Jackson Laboratory) were used. Formalin injection was done by injecting 30–40 μL of 2% paraformaldehyde into the plantar surface of the hindpaw. Rotarod testing was done with a standard program accelerating from 0 to 40 rotations per minute over 5 min.

Nuclei Preparation

This protocol was adapted from Halder et al. (2016). Animals were euthanized by CO_2 inhalation, the lumbar spinal cord was rapidly dissected, and dorsal root ganglia were removed. The cords were dounced in 500 μL of sucrose buffer (0.32 M sucrose, 10 mM HEPES [pH 8.0], 5 mM $CaCl_2$, 3 mM Mg-acetate, 0.1 mM EDTA, 1 mM DTT) with 0.1% Triton X-100 using five strokes with the A pestle (Kontes Dounce Tissue Grinder) followed by five strokes with the B pestle. The lysate was then diluted with 3 mL of sucrose buffer and was centrifuged at 3,200 × *g* for 10 min. The supernatant was removed, and 3 mL of sucrose buffer was added to the pellet and incubated for 1–2 min; the loosened pellet was then transferred to an Oak Ridge centrifuge tube. The pellet was then homogenized using Ultra-Turrax on setting 1 for 1 min. 12 mL of density buffer (1 M sucrose, 10 mM HEPES [pH 8.0], 3 mM Mg-acetate, 1 mM DTT) was then added carefully below the nuclei layer, and the tube was centrifuged at 3,200 × *g* for 20 min. The supernatant was then rapidly poured off, and the nuclei on the walls of the tube were collected with 1 mL of PBS with 0.02% BSA and spun at 3,200 × *g* for 10 min. Nuclei were then resuspended in PBS with 0.02% BSA.

Drop-Seq and Analysis

Each Drop-Seq sample was produced from the lumbar cords of a pair of ICR mice 8–12 weeks old. There were nine independent samples for baseline (four male and five female), five independent samples for formalin treatment (three male and two female), and five independent samples for rotarod behavior (three male and two female).

The Drop-Seq method was performed as previously described (Macosko et al., 2015) except that the following concentrations were used: 225 nuclei/μL, 250 beads/μL, and 0.7% sarkosyl in the lysis buffer; flow rates were adjusted accordingly. Clustering was performed using SC3 consensus clustering (Kiselev et al., 2017). All antibodies and *in situ* hybridization probes used for validation are listed in Table S4.

DATA AND SOFTWARE AVAILABILITY

The accession number for the raw sequencing data reported in this paper is GEO: GSE103892.

SUPPLEMENTAL INFORMATION

Supplemental Information includes Supplemental Experimental Procedures, four figures, and four tables and can be found with this article online at https://doi.org/10.1016/j.celrep.2018.02.003.

ACKNOWLEDGMENTS

Human adult spinal cord tissues were procured by the National Disease Research Interchange (NDRI) with support from NIH grant 2 U42 OD011158 and the assistance of Dr. Christopher Grunseich and Dr. Kenneth Fischbeck. We thank Dr. Arnab Barik for expertise and assistance with *in situ* hybridization, Dr. Alexander Chesler for sharing reagents, and Dr. Yuesheng Li for expertise and assistance with sequencing. The Lbx1 antibody was a gift of Dr. Carmen Birchmeier. This research was supported by NIH Intramural Research Program funding from the NINDS (1 ZIA NS003153 02 to A.S., K.R.J., L.L., K.J.E.M., C.I.D., A.R.R., T.B.B., and A.J.L.) and the NIDCD (1 ZIA DC000059 18 to M.C.K. and M.W.K.).

AUTHOR CONTRIBUTIONS

A.S. and A.J.L. conceived the project. K.R.J. performed all bio-informatic analysis. K.J.E.M., M.C.K., and A.J.L. performed Drop-Seq experiments. A.S., L.L., A.R.R., T.B.B., and C.I.D. performed validation experiments. A.S., K.R.J., K.J.E.M., M.C.K., M.W.K., and A.J.L. analyzed experiments. A.S., K.R.J., and A.J.L. wrote the manuscript.

DECLARATION OF INTERESTS

The authors declare no competing interests.

Received: September 13, 2017
Revised: December 19, 2017
Accepted: January 30, 2018
Published: February 20, 2018

REFERENCES

Abraira, V.E., Kuehn, E.D., Chirila, A.M., Springel, M.W., Toliver, A.A., Zimmerman, A.L., Orefice, L.L., Boyle, K.A., Bai, L., Song, B.J., et al. (2017). The cellular and synaptic architecture of the mechanosensory dorsal horn. Cell *168*, 295–310.e19.

Alvarez, F.J., Jonas, P.C., Sapir, T., Hartley, R., Berrocal, M.C., Geiman, E.J., Todd, A.J., and Goulding, M. (2005). Postnatal phenotype and localization of spinal cord V1 derived interneurons. J. Comp. Neurol. *493*, 177–192.

Azim, E., Jiang, J., Alstermark, B., and Jessell, T.M. (2014). Skilled reaching relies on a V2a propriospinal internal copy circuit. Nature *508*, 357–363.

Bikoff, J.B., Gabitto, M.I., Rivard, A.F., Drobac, E., Machado, T.A., Miri, A., Brenner-Morton, S., Famojure, E., Diaz, C., Alvarez, F.J., et al. (2016). Spinal inhibitory interneuron diversity delineates variant motor microcircuits. Cell *165*, 207–219.

Bourane, S., Grossmann, K.S., Britz, O., Dalet, A., Del Barrio, M.G., Stam, F.J., Garcia-Campmany, L., Koch, S., and Goulding, M. (2015). Identification of a spinal circuit for light touch and fine motor control. Cell *160*, 503–515.

Campbell, J.N., Macosko, E.Z., Fenselau, H., Pers, T.H., Lyubetskaya, A., Tenen, D., Goldman, M., Verstegen, A.M.J., Resch, J.M., McCarroll, S.A.,

et al. (2017). A molecular census of arcuate hypothalamus and median eminence cell types. Nat. Neurosci. *20*, 484–496.

Catela, C., Shin, M.M., and Dasen, J.S. (2015). Assembly and function of spinal circuits for motor control. Annu. Rev. Cell Dev. Biol. *31*, 669–698.

Chen, R., Wu, X., Jiang, L., and Zhang, Y. (2017). Single-cell RNA-seq reveals hypothalamic cell diversity. Cell Rep. *18*, 3227–3241.

Crone, S.A., Quinlan, K.A., Zagoraiou, L., Droho, S., Restrepo, C.E., Lundfald, L., Endo, T., Setlak, J., Jessell, T.M., Kiehn, O., and Sharma, K. (2008). Genetic ablation of V2a ipsilateral interneurons disrupts left-right locomotor coordination in mammalian spinal cord. Neuron *60*, 70–83.

Dougherty, K.J., Zagoraiou, L., Satoh, D., Rozani, I., Doobar, S., Arber, S., Jessell, T.M., and Kiehn, O. (2013). Locomotor rhythm generation linked to the output of spinal shox2 excitatory interneurons. Neuron *80*, 920–933.

Duan, B., Cheng, L., Bourane, S., Britz, O., Padilla, C., Garcia-Campmany, L., Krashes, M., Knowlton, W., Velasquez, T., Ren, X., et al. (2014). Identification of spinal circuits transmitting and gating mechanical pain. Cell *159*, 1417–1432.

Francius, C., Harris, A., Rucchin, V., Hendricks, T.J., Stam, F.J., Barber, M., Kurek, D., Grosveld, F.G., Pierani, A., Goulding, M., et al. (2013). Identification of multiple subsets of ventral interneurons and differential distribution along the rosstrocaudal axis of the developing spinal cord. PLoS One *8*, e70325.

Galtrey, C.M., Kwok, J.C.F., Carulli, D., Rhodes, K.E., and Fawcett, J.W. (2008). Distribution and synthesis of extracellular matrix proteoglycans, hyaluronan, link proteins and tenascin-R in the rat spinal cord. Eur. J. Neurosci. *27*, 1373–1390.

Gong, S., Zheng, C., Doughty, M.L., Losos, K., Didkovsky, N., Schambra, U.B., Nowak, N.J., Joyner, A., Leblanc, G., Hatten, M.E., and Heintz, N. (2003). A gene expression atlas of the central nervous system based on bacterial artificial chromosomes. Nature *425*, 917–925.

Grindberg, R.V., Yee-Greenbaum, J.L., McConnell, M.J., Novotny, M., O'Shaughnessy, A.L., Lambert, G.M., Araúzo-Bravo, M.J., Lee, J., Fishman, M., Robbins, G.E., et al. (2013). RNA-sequencing from single nuclei. Proc. Natl. Acad. Sci. USA *110*, 19802–19807.

Habib, N., Li, Y., Heidenreich, M., Swiech, L., Avraham-Davidi, I., Trombetta, J.J., Hession, C., Zhang, F., and Regev, A. (2016). Div-Seq: Single-nucleus RNA-Seq reveals dynamics of rare adult newborn neurons. Science *353*, 925–928.

Habib, N., Avraham-Davidi, I., Basu, A., Burks, T., Shekhar, K., Hofree, M., Choudhury, S.R., Aguet, F., Gelfand, E., Ardlie, K., et al. (2017). Massively parallel single-nucleus RNA-seq with DroNc-seq. Nat. Methods *14*, 955–958.

Halder, R., Hennion, M., Vidal, R.O., Shomroni, O., Rahman, R.U., Rajput, A., Centeno, T.P., van Bebber, F., Capece, V., Garcia Vizcaino, J.C., et al. (2016). DNA methylation changes in plasticity genes accompany the formation and maintenance of memory. Nat. Neurosci. *19*, 102–110.

Hayashi, M., Hinckley, C.A., Driscoll, S.P., Moore, N.J., Levine, A.J., Hilde, K.L., Sharma, K., and Pfaff, S.L. (2018). Graded arrays of spinal and supraspinal V2a interneuron subtypes underlie forelimb and hindlimb motor control. Neuron, Published online February 1, 2018. https://doi.org/10.1016/j.neuron.2018.01.023.

Herdegen, T., Rüdiger, S., Mayer, B., Bravo, R., and Zimmermann, M. (1994). Expression of nitric oxide synthase and colocalisation with Jun, Fos and Krox transcription factors in spinal cord neurons following noxious stimulation of the rat hindpaw. Brain Res. Mol. Brain Res. *22*, 245–258.

Hilde, K.L., Levine, A.J., Hinckley, C.A., Hayashi, M., Montgomery, J.M., Gullo, M., Driscoll, S.P., Grosschedl, R., Kohwi, Y., Kohwi-Shigematsu, T., and Pfaff, S.L. (2016). Satb2 is required for the development of a spinal exteroceptive microcircuit that modulates limb position. Neuron *91*, 763–776.

Hossaini, M., Duraku, L.S., Saraç, C., Jongen, J.L.M., and Holstege, J.C. (2010). Differential distribution of activated spinal neurons containing glycine and/or GABA and expressing c-fos in acute and chronic pain models. Pain *151*, 356–365.

Hrvatin, S., Hochbaum, D.R., Nagy, M.A., Cicconet, M., Robertson, K., Cheadle, L., Zilionis, R., Ratner, A., Borges-Monroy, R., Klein, A.M., et al. (2018). Single-cell analysis of experience-dependent transcriptomic states in the mouse visual cortex. Nat. Neurosci. *21*, 120–129.

Huang, A., Noga, B.R., Carr, P.A., Fedirchuk, B., and Jordan, L.M. (2000). Spinal cholinergic neurons activated during locomotion: localization and electrophysiological characterization. J. Neurophysiol. *83*, 3537–3547.

Jaitin, D.A., Kenigsberg, E., Keren-Shaul, H., Elefant, N., Paul, F., Zaretsky, I., Mildner, A., Cohen, N., Jung, S., Tanay, A., and Amit, I. (2014). Massively parallel single-cell RNA-seq for marker-free decomposition of tissues into cell types. Science *343*, 776–779.

Jasmin, L., Gogas, K.R., Ahlgren, S.C., Levine, J.D., and Basbaum, A.I. (1994). Walking evokes a distinctive pattern of Fos-like immunoreactivity in the caudal brainstem and spinal cord of the rat. Neuroscience *58*, 275–286.

Kiselev, V.Y., Kirschner, K., Schaub, M.T., Andrews, T., Yiu, A., Chandra, T., Natarajan, K.N., Reik, W., Barahona, M., Green, A.R., and Hemberg, M. (2017). SC3: consensus clustering of single cell RNA-seq data. Nat. Methods *14*, 483–486.

Koch, S.C., Acton, D., and Goulding, M. (2017a). Spinal circuits for touch, pain, and itch. Annu. Rev. Physiol. Published online September 27, 2017. https://doi.org/10.1146/annurev-physiol-022516-034303.

Koch, S.C., Del Barrio, M.G., Dalet, A., Gatto, G., Günther, T., Zhang, J., Seidler, B., Saur, D., Schüle, R., and Goulding, M. (2017b). RORβ spinal interneurons gate sensory transmission during locomotion to secure a fluid walking gait. Neuron *96*, 1419–1431.e5.

Lacar, B., Linker, S.B., Jaeger, B.N., Krishnaswami, S.R., Barron, J.J., Kelder, M.J., Parylak, S.L., Paquola, A.C., Venepally, P., Novotny, M., et al. (2016). Nuclear RNA-seq of single neurons reveals molecular signatures of activation. Nat. Commun. *7*, 1–12.

Lake, B.B., Ai, R., Kaeser, G.E., Salathia, N.S., Yung, Y.C., Liu, R., Wildberg, A., Gao, D., Fung, H.-L., Chen, S., et al. (2016). Neuronal subtypes and diversity revealed by single-nucleus RNA sequencing of the human brain. Science *352*, 1586–1590.

Lake, B.B., Codeluppi, S., Yung, Y.C., Gao, D., Chun, J., Kharchenko, P.V., Linnarsson, S., and Zhang, K. (2017). A comparative strategy for single-nucleus and single-cell transcriptomes confirms accuracy in predicted cell-type expression from nuclear RNA. Sci. Rep. *7*, 6031.

Laplante, M., and Sabatini, D.M. (2012). mTOR signaling in growth control and disease. Cell *149*, 274–293.

Lee, J.H., Price, R.H., Williams, F.G., Mayer, B., and Beitz, A.J. (1993). Nitric oxide synthase is found in some spinothalamic neurons and in neuronal processes that appose spinal neurons that express Fos induced by noxious stimulation. Brain Res. *608*, 324–333.

Lein, E.S., Hawrylycz, M.J., Ao, N., Ayres, M., Bensinger, A., Bernard, A., Boe, A.F., Boguski, M.S., Brockway, K.S., Byrnes, E.J., et al. (2007). Genome-wide atlas of gene expression in the adult mouse brain. Nature *445*, 168–176.

Li, C.-L., Li, K.-C., Wu, D., Chen, Y., Luo, H., Zhao, J.-R., Wang, S.-S., Sun, M.-M., Lu, Y.-J., Zhong, Y.-Q., et al. (2016). Somatosensory neuron types identified by high-coverage single-cell RNA-sequencing and functional heterogeneity. Cell Res. *26*, 83–102.

Lu, D.C., Niu, T., and Alaynick, W.A. (2015). Molecular and cellular development of spinal cord locomotor circuitry. Front. Mol. Neurosci. *8*, 25.

Macosko, E.Z., Basu, A., Satija, R., Nemesh, J., Shekhar, K., Goldman, M., Tirosh, I., Bialas, A.R., Kamitaki, N., Martersteck, E.M., et al. (2015). Highly parallel genome-wide expression profiling of individual cells using nanoliter droplets. Cell *161*, 1202–1214.

Matevossian, A., and Akbarian, S. (2008). Neuronal nuclei isolation from human postmortem brain tissue. J. Vis. Exp. *20*, e914.

Mishra, S.K., and Hoon, M.A. (2013). The cells and circuitry for itch responses in mice. Science *340*, 968–971.

Neumann, S., Braz, J.M., Skinner, K., Llewellyn-Smith, I.J., and Basbaum, A.I. (2008). Innocuous, not noxious, input activates PKCgamma interneurons of the spinal dorsal horn via myelinated afferent fibers. J. Neurosci. *28*, 7936–7944.

Peirs, C., Williams, S.-P.G., Zhao, X., Walsh, C.E., Gedeon, J.Y., Cagle, N.E., Goldring, A.C., Hioki, H., Liu, Z., Marell, P.S., and Seal, R.P. (2015). Dorsal horn circuits for persistent mechanical pain. Neuron *87*, 797–812.

Perry, S., Gezelius, H., Larhammar, M., Hilscher, M.M., Lamotte d'Incamps, B., Leao, K.E., and Kullander, K. (2015). Firing properties of Renshaw cells defined by Chrna2 are modulated by hyperpolarizing and small conductance ion currents Ih and ISK. Eur. J. Neurosci. *41*, 889–900.

Polgár, E., Sardella, T.C.P., Tiong, S.Y.X., Locke, S., Watanabe, M., and Todd, A.J. (2013). Functional differences between neurochemically defined populations of inhibitory interneurons in the rat spinal dorsal horn. Pain *154*, 2606–2615.

Satoh, D., Pudenz, C., and Arber, S. (2016). Context-dependent gait choice elicited by EphA4 mutation in Lbx1 spinal interneurons. Neuron *89*, 1046–1058.

Seredick, S., Hutchinson, S.A., Van Ryswyk, L., Talbot, J.C., and Eisen, J.S. (2014). Lhx3 and Lhx4 suppress Kolmer-Agduhr interneuron characteristics within zebrafish axial motoneurons. Development *141*, 3900–3909.

Shin, J., Berg, D.A., Zhu, Y., Shin, J.Y., Song, J., Bonaguidi, M.A., Enikolopov, G., Nauen, D.W., Christian, K.M., Ming, G.-L., and Song, H. (2015). Single-cell RNA-seq with waterfall reveals molecular cascades underlying adult neurogenesis. Cell Stem Cell *17*, 360–372.

Sun, Y.-G., Zhao, Z.-Q., Meng, X.-L., Yin, J., Liu, X.-Y., and Chen, Z.-F. (2009). Cellular basis of itch sensation. Science *325*, 1531–1534.

Sweeney, L.B., Bikoff, J.B., Gabitto, M.I., Brenner-Morton, S., Baek, M., Yang, J.H., Tabak, E.G., Dasen, J.S., Kintner, C.R., and Jessell, T.M. (2018). Origin and segmental diversity of spinal inhibitory interneurons. Neuron *97*, 341–355.e3.

Tasic, B., Menon, V., Nguyen, T.N., Kim, T.K., Jarsky, T., Yao, Z., Levi, B., Gray, L.T., Sorensen, S.A., Dolbeare, T., et al. (2016). Adult mouse cortical cell taxonomy revealed by single cell transcriptomics. Nat. Neurosci. *19*, 335–346.

Todd, A.J. (2017). Identifying functional populations among the interneurons in laminae I–III of the spinal dorsal horn. Mol. Pain *13*, 1744806917693003.

Tripathy, S.J., Toker, L., Li, B., Crichlow, C.-L., Tebaykin, D., Mancarci, B.O., and Pavlidis, P. (2017). Transcriptomic correlates of neuron electrophysiological diversity. PLoS Comput. Biol. *13*, e1005814.

Usoskin, D., Furlan, A., Islam, S., Abdo, H., Lönnerberg, P., Lou, D., Hjerling-Leffler, J., Haeggström, J., Kharchenko, O., Kharchenko, P.V., et al. (2015). Unbiased classification of sensory neuron types by large-scale single-cell RNA sequencing. Nat. Neurosci. *18*, 145–153.

Villani, A.C., Satija, R., Reynolds, G., Sarkizova, S., Shekhar, K., Fletcher, J., Griesbeck, M., Butler, A., Zheng, S., Lazo, S., et al. (2017). Single-cell RNA-seq reveals new types of human blood dendritic cells, monocytes, and progenitors. Science *356*, eaah4573.

Wu, Y.E., Pan, L., Zuo, Y., Li, X., and Hong, W. (2017). Detecting activated cell populations using single-cell RNA-seq. Neuron *96*, 313–329.e6.

Zagoraiou, L., Akay, T., Martin, J.F., Brownstone, R.M., Jessell, T.M., and Miles, G.B. (2009). A cluster of cholinergic premotor interneurons modulates mouse locomotor activity. Neuron *64*, 645–662.

Zhang, J., Lanuza, G.M., Britz, O., Wang, Z., Siembab, V.C., Zhang, Y., Velasquez, T., Alvarez, F.J., Frank, E., and Goulding, M. (2014). V1 and v2b interneurons secure the alternating flexor-extensor motor activity mice require for limbed locomotion. Neuron *82*, 138–150.

Cell Reports, Volume *22*

Supplemental Information

Massively Parallel Single Nucleus Transcriptional Profiling Defines Spinal Cord Neurons and Their Activity during Behavior

Anupama Sathyamurthy, Kory R. Johnson, Kaya J.E. Matson, Courtney I. Dobrott, Li Li, Anna R. Ryba, Tzipporah B. Bergman, Michael C. Kelly, Matthew W. Kelley, and Ariel J. Levine

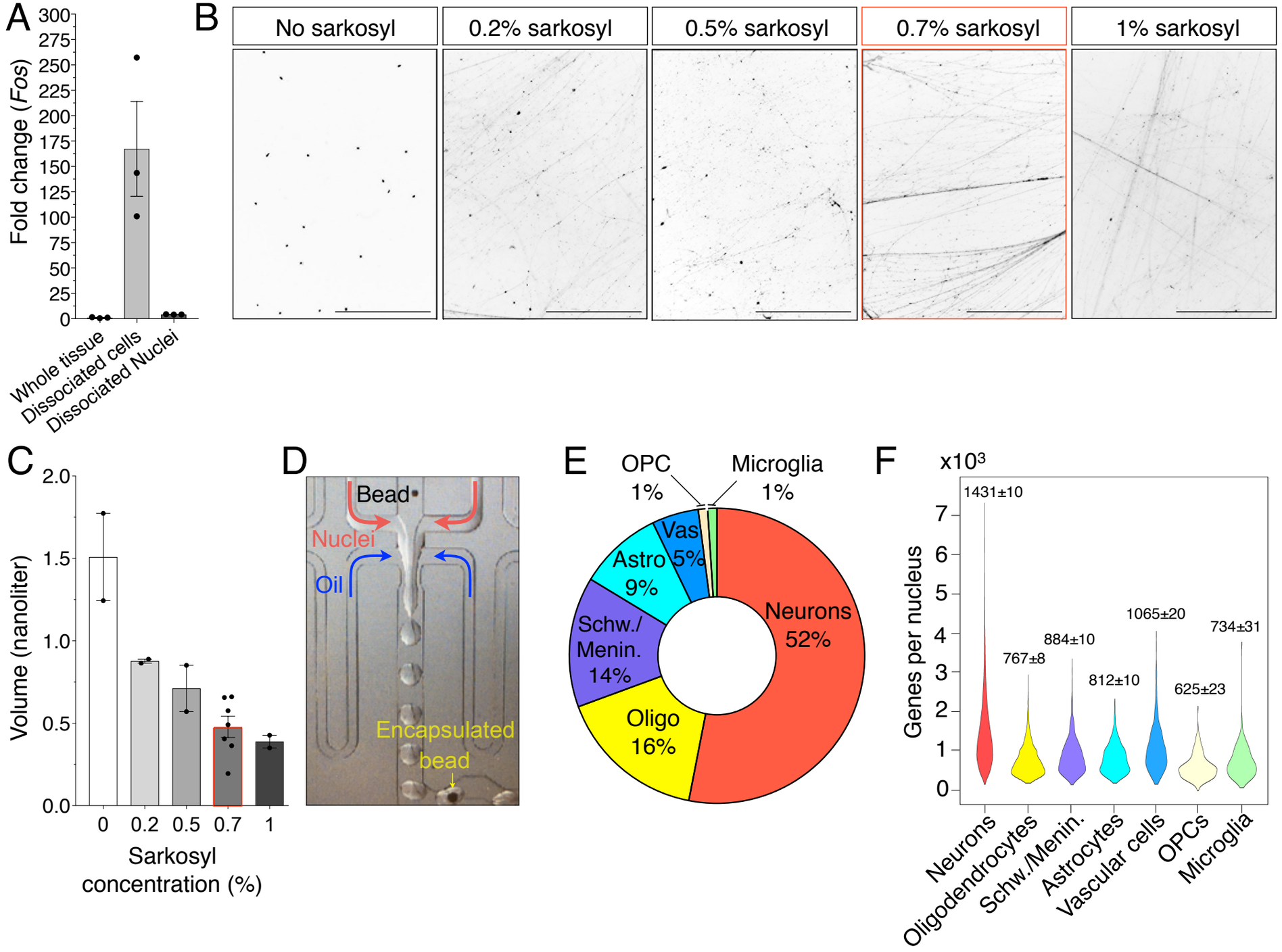

Figure S1. Characterization of the massively parallel single nucleus RNA-seq approach to identify spinal cord cell types. Related to Figure 1. Characterization of the massively parallel single nucleus RNA-seq approach to identify spinal cord cell types. (A) RT-qPCR detection of *Fos* RNA from whole spinal cord tissue, dissociated cells, and dissociated nuclei (normalized to *Gapdh*, performed from three independent biological samples for each). Mean ± s.e.m. are shown. (B) DNA visualized with DAPI stain from isolated nuclei in lysis buffer containing varying concentrations of the detergent sarkosyl. 0.7% sarkosyl was selected for further experiments. Scale bars are 500 μm. (C) Droplet volume with varying concentrations of sarkosyl. Mean ± s.e.m. are shown. (D) Drop-Seq apparatus image showing bead inflow, nuclei inflow, and oil inflow, as well as the formation of droplets and the encapsulation of beads. (E) Pie chart showing the overall contribution of each major cell type to the total population of 17,354 nuclei: Neurons, Oligodendrocytes (Oligo), Meningeal/Schwann cells (Menin./Schw.), Astrocytes (Astro), Vascular cells (Vas), Oligodendrocyte precursor cells (OPC), and Microglia. (F) Genes detected per nucleus, by major cell type. A violin plot distribution is shown, as well as the mean ± s.e.m.

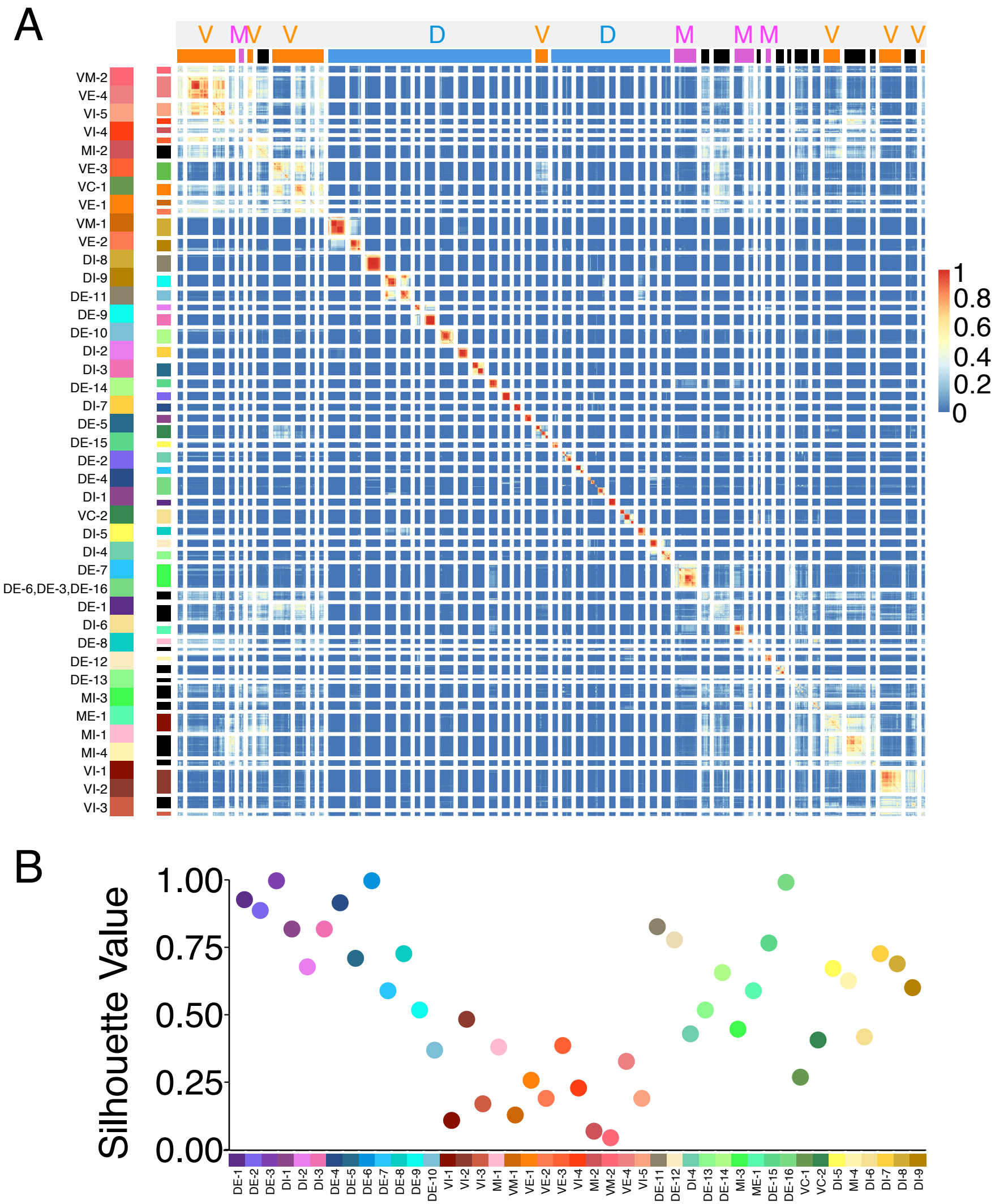

Figure S2. Cluster consensus metrics. Related to Figure 2. (A) Nucleus-by-nucleus consensus matrix based on co-clustering within SC3. Consensus is measured on a scale from 0 (blue) to 1 (red). Fifty-two clusters are shown, including those that were discarded (see Experimental Procedures; black). Clusters DE-3, DE-6, and DE-16 were obtained by sub-clustering the indicated cluster. The spatial location of each cluster is shown on top (D – dorsal, V – ventral, M – intermediate zone/deep dorsal/"mid"). Note that the cluster order is distinct from other figures and is shown on the left. (B) Silhouette width consensus values, plotted by cluster for the final set of forty-three clusters. This measure represents the "diagonality" of the consensus matrix.

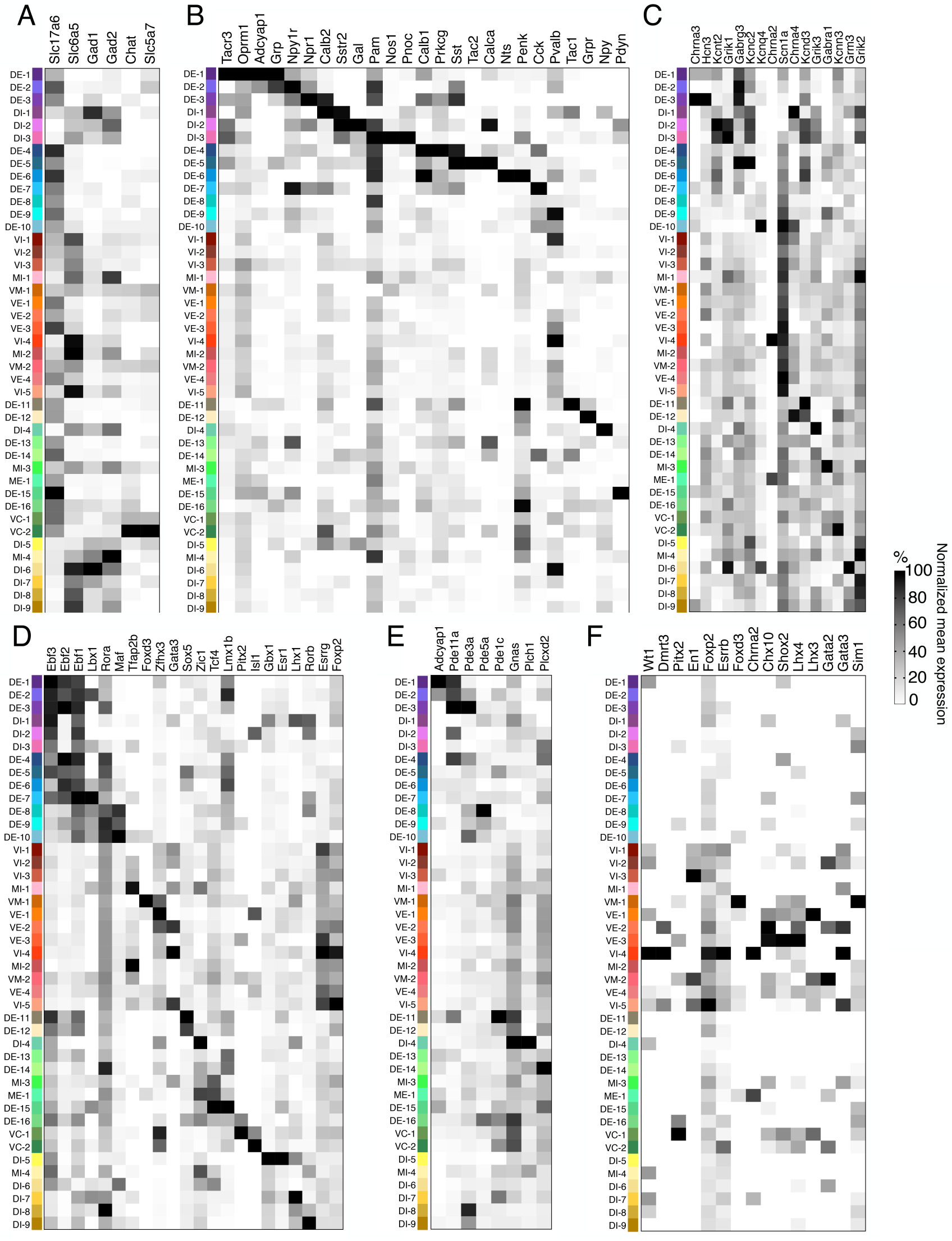

Figure S3. Gene expression across clusters. Related to Figures 2 and 3. (A) Normalized mean gene expression for neurotransmitter markers using excitatory marker *Slc17a6*/vGlut2, inhibitory markers *Slc6a5*/GlyT2 (glycinergic), *Gad1* (gaba-ergic), and *Gad2* (gaba-ergic), and cholinergic markers *Chat* and *Slc5a7*/CHT. (B-F) Normalized mean gene expression across clusters for genes that are classic spinal cord markers (B), neurotransmitter receptors and channel proteins (C), transcription factors (D), cAMP pathway components (defined by GO analysis) (E), and embryonic-lineage domain markers (F).

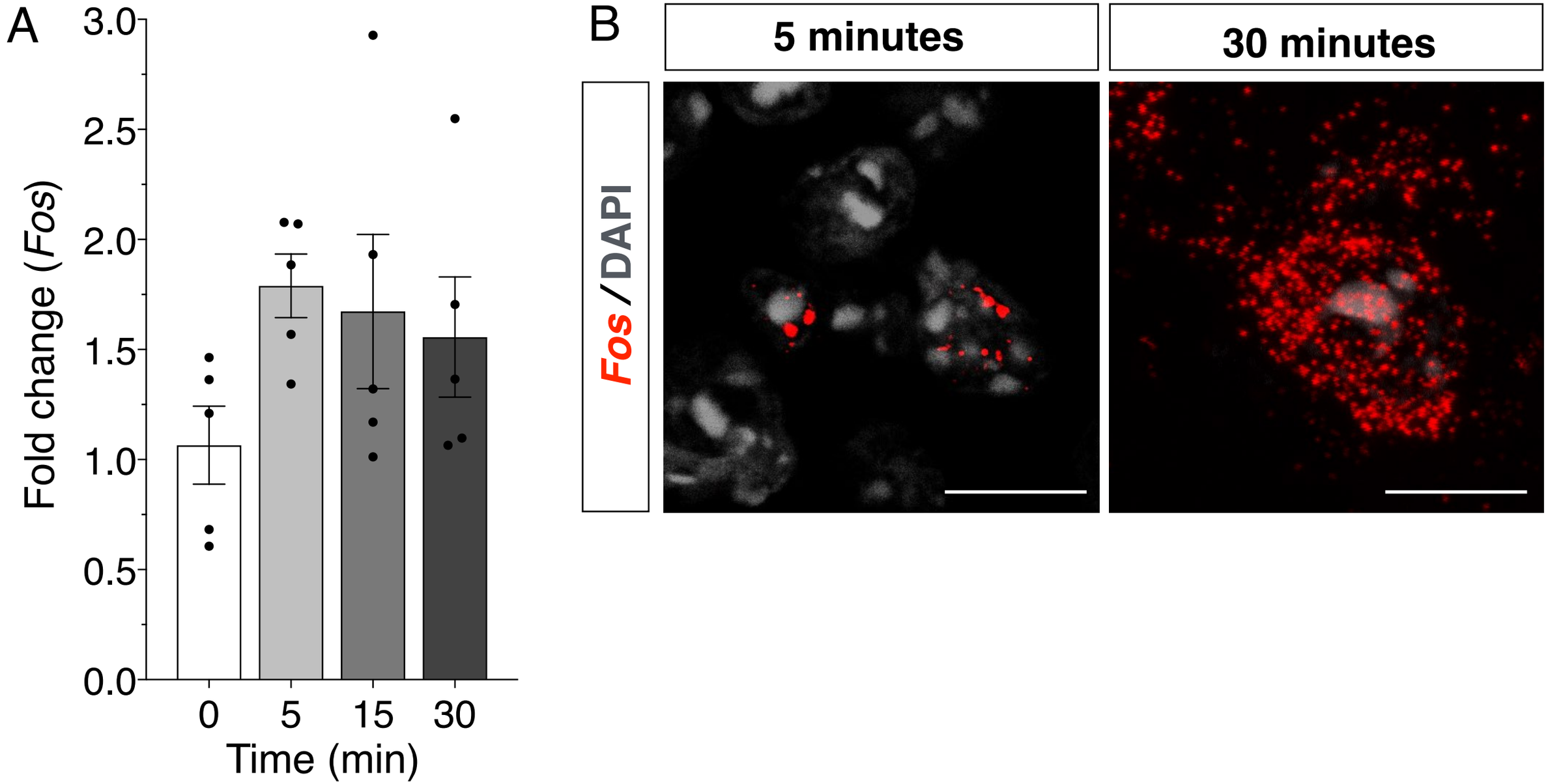

Figure S4. *Fos* mRNA detected in nuclei following formalin administration. Related to Figure 5. *Fos* mRNA detected in nuclei following formalin administration. (A) Fos mRNA as detected by RT-qPCR from bulk nuclei isolated following formalin administration at 0, 5, 15, or 30 minutes. mRNA levels are presented as fold-change from baseline, after normalization to *Gapdh* levels. Five independent biological samples were analyzed for each time point. Mean ± s.e.m are shown. (B) Fos mRNA as detected by fluorescent in situ hybridization at 5 minutes (left) and 30 minutes (right) following formalin administration, showing sub-cellular distribution of mRNA. Scale bars are 10 μm.

SUPPLEMENTAL TABLES

Table S1. Related to Figure 1. All genes significantly associated with non-neuronal clusters.

Table S2. Related to Figure 2. All genes significantly associated with neuronal clusters.

Table S3. Related to Main Text descriptions of clusters and Figures 2-4. Gene expression within each cluster for all detected genes, presented as the mean gene expression of each gene in each cluster and the percent of nuclei in each cluster that express the indicated gene.

Reagent	Source	Catalog	Antibody dilution/RNA	Usage Notes
Cacna1e	ACD	449211	RNA	
cFOS-Gt	Santa Cruz Biotechnology	sc-52-G	1:500	
cFOS-Rb	Santa Cruz Biotechnology	sc-52	1:500	
Chx10	Santa Cruz Biotechnology	sc-8047	1:500	
FOS	ACD	316921	RNA	
Ebf1	EMDMillipore	AB10523	1:500	antigen retrieval
Ebf2	R&D Systems	AF7006	1:500	
Grik3	ACD	493981 (HS)	RNA	
Lbx1	gift of C. Birchmeier	N/A	1:10,000	
Necab1	ACD	428541-C2	RNA	
Nrgn	R&D Systems	MAB7947-SP	01:50	
Npy	ACD	313321-C2	RNA	
PKCg	Santa Cruz Biotechnology	sc-211	1:500	
Rorb	ACD	444271	RNA	
Satb1	Santa Cruz Biotechnology	sc-376096	1:500	
Snca	ACD	313281	RNA	
Syt1	ACD	491831	RNA	

Table S4. Related to Experimental Procedures. Antibodies and RNA probes used in validation.

SUPPLEMENTAL EXPERIMENTAL PROCEDURES

Single Cell Dissociation. Cells were dissociated using the Miltenyi Neural Dissociation Kit (P) (130-092-628), with manual dissociation according to the manufacturer's protocol.

Bulk Nuclei RT-qPCR. Three samples (one animal each) were used for Figure S1A. Five samples (one animal each) were analyzed for each time point in Figure S4A. Nuclei or cells were prepared as above, then spun at 3,200xg for 10 minutes. The supernatant was removed and 350 μl of buffer RLT (Qiagen RNeasy Mini Kit) was used for lysis. Total RNA was then extracted using the Qiagen RNeasy Mini Kit, including on-column DNase digestion. cDNA (and a no RT control) was prepared using SuperScript IV First-Strand Synthesis System and qPCR (with technical triplicates for each sample) was performed using the following primers. cFOS_F: CTGAGAAGACTGGATAGAGC; cFOS_R: CGTTGAAACCCGAGAACATC; Gapdh_F: AGGTCGGTGTGAACGGATTTG; Gapdh_R: GGGGTCGTTGATGGCAACA.

Drop-Seq: For sample preparation, nuclei in 1mL of PBS with 0.02% BSA were counted with a hemocytometer and adjusted to a final concentration of 225 nuclei/μl. Beads (Chemgenes, Macosko-2011-10, lot 011717C) were prepared at a concentration of 250 beads/μl. Lysis buffer detergent concentration was adjusted to 0.7% sarkosyl. For the apparatus, a PDMS device from FlowJem was used (according to the Drop-Seq CAD design), CorSolutions pumps were used to replace syringe pumps for the cell and oil lines, and the flow was visually monitored using a Photronics High Speed camera (5000 frames per second). The following flow rates were used: beads (35μl/min), nuclei (35 μl/min), oil (200 μl/min). We analyzed individual droplets to characterize the bead occupancy and droplet size that result from these new parameters (n = 581 droplets from 5 samples). We found that 5.7 ± 1% (s.e.m.) of droplets contained a bead, all droplets with beads had a single bead, and the calculated droplet size was 0.46 ± 0.08 nl (s.e.m.). Droplet volume was calculated as the % droplet occupancy divided by 125 beads/μl (which was one half of the initial bead concentration).

For the cDNA amplification and library preparation, multiple PCR reactions were performed for each sample, pooled, purified with AMPure beads (0.6X), quantified with Qubit 3.0, and analyzed on a High Sensitivity DNA Bioanalyzer chip. Multiple tagmentation and library preparation reactions were performed for each sample, each with 600 pg input. Parallel reactions were then pooled, double purified with AMPure beads (0.8X), quantified with Qubit 3.0, and analyzed on a High Sensitivity DNA Bioanalyzer chip. Libraries were sequenced at a minimum depth of 20,000 reads per nucleus using HiSeq 2500 Rapid Mode with the following parameters. Read 1: 25bp, index, custom primer; Read 2: 50bp, Illumina primer.

snRNA-Seq Data Processing. Raw sequence reads (.fastq) per sample were pre-processed, mapped against MM10, and the number of mapped reads per gene enumerated (exon+intron) by cell barcode using commands described in the "Drop-seq Alignment Cookbook" (http://mccarrolllab.com/Drop-Seq/). Quality inspection and filtering of the count data returned was performed using functions supported in the "scater" package (https://bioconductor.org/packages/release/bioc/html/scater.html). First, metrics for

mitochondrial (MT) genes per cell barcode were generated using the calculateQCMetrics() function then inspected using the hist() and scater::plotPhenoData() functions. Among the metrics generated per cell barcode was the percent total reads mapped to MT genes. This specific metric was next used to filter-discard nuclei with a percent total reads mapped to MT genes $\geq$ 20%. For surviving cell barcodes/nuclei, MT read counts and immediate early genes were filter-removed and metrics generated for remaining genes by nuclei using the same calculateQCMetrics() function. Among these metrics generated was the total number of genes with mapped reads per nuclei and the total number of mapped reads across genes per nuclei. These two metrics were inspected using the same hist() and scater::plotPhenoData() functions used prior and threshold filters defined to discard outlier nuclei. Specifically, nuclei having $\leq$ 200 genes per nucleus were discarded. During sub-clustering of the neuronal populations, nuclei having $\leq$ 500 genes per nucleus were discarded.

snRNA-Seq Clustering and Analysis. For clustering, the "SC3" package (https://bioconductor.org/packages/release/bioc/html/SC3.html) was used on normalized expression for nuclei not discarded in these two successive steps. The normalization method used was "Counts Per Million"; also referred to as "CPM". All genes in $\geq$ 3 nuclei were analyzed and the gene filter was set to “false”. The first clustering in SC3 step involved ten clusters, while seven clusters were considered further. One cluster was excluded because it was considered to contain low quality nuclei and was not defined by any cell-type specific genes, but rather by genes from a list of the twenty genes with the most mapped reads in the entire set. Two small clusters were discarded because they contained < 0.5% of the total nuclei. We verified that all clusters contained nuclei from at least three biological samples. To visualize SC3-derived clusters of nuclei by t-SNE scatterplot, CPM expression of detected genes expressed across nuclei were passed to the Rtsne() function under default settings and the results returned passed to the plot() function. The second-clustering step was performed on the neuronal nuclei (cluster 1) obtained by SC3 analysis of the total set of nuclei. Preliminary SC3 analysis identified a cluster of low quality nuclei and a cluster that represented doublets between nuclei from neurons and oligodendrocytes and both of these clusters were discarded from further analysis. SC3 analysis of the remaining nuclei then identified fifty-two clusters. The complete fifty-two cluster set can be seen in Figure S2A. This set of clusters was determined through an iterative process of clustering, followed by visual inspection of gene lists and comparison to established spinal cord markers. At this step, clusters that represented doublets, that did not have at least three significantly associated annotated genes, or that contained less than 0.7% of the total neuronal nuclei were discarded from further analysis. These discarded clusters are indicated by black bars in Figure S2A. After these exclusions, there were forty-one remaining clusters. One cluster (#30 in the original analysis) was further sub-clustered, following inspection of the tSNE plot and cell consensus matrix, which suggested three sub-groups that were not related to each other. Thus, a final list of forty-three clusters was analyzed. All of these clusters had nuclei from at least three independent biological samples. To assess relatedness of clustered nuclei, the mean expression per gene (with CPM expression > 0) per cluster was calculated in R and then passed to the dist() function to produce a Euclidean-based distance metric for each pair-wise combination of clusters. These distance metrics were then used in the performance of hierarchical clustering using “complete” agglomeration via the hclust() function. The

dendrogram describing the results of how clusters of nuclei are related was visualized via the as.phylo() function. GO term analysis was performed using GO David Functional Annotation Tool with the top ten most significant genes for each cluster, using functional annotation clustering on “molecular function” GO terms with low stringency. Functional annotation groupings with an enrichment score > 1.3 (-log of mean p-value) are presented.

Immunofluorescence. Animals were euthanized with avertin either at baseline or one hour after behavior and perfused with PBS and 4% paraformaldehyde. Lumbar spinal cords were extracted and washed in PBS, incubated overnight in 30% sucrose, and embedded in OCT. Frozen sections of 50 μm were cut and stained, using a blocking buffer that contained 1% IgG-free BSA, 10% donkey serum, and 0.1% Triton-X 100 in PBS. Antibodies used are presented in Table S4. At least eight sections from at least two male and two female animals, ages 8-12 weeks old, were analyzed for expression patterns and a representative example was imaged by confocal microscopy (Zeiss 800 LSM).

In Situ Hybridization. Animals were euthanized by cervical dislocation at baseline or thirty minutes after behavior and the lumbar spinal cords were extracted and fresh frozen in OCT. Frozen sections of 16-18 μm were cut and RNAscope (ACD) was used for in situ hydridization using the manufacturer’s protocol. Probes used are presented in Table S4. At least five sections from at least two male and two female animals, ages 8-12 weeks old, were analyzed for expression patterns and a representative example was imaged by confocal microscopy (Zeiss 800 LSM).